Chapter 1

Computer Implementation of Hydro-Mechnical Model

1.1 Computer implementation of hypoplastic model and test benchmarks

1.1.1 Isothermal water flow in deforming medium

A fully coupled thermo-hygro-mechanical approach is simplified assuming the liquid water transfer as the only driving mechanism for isothermal saturation processes in soils. The effects of pore gas pressure and temperature are neglected in the governing system of Equations [Schrefler and Lewis, 1998]. The final system of Equations is simplified into the following fully-coupled form

$$\begin{pmatrix} \boldsymbol{K}_{uu} & \boldsymbol{K}_{uw} \\ \boldsymbol{0} & \boldsymbol{K}_{ww} \end{pmatrix} \begin{pmatrix} \boldsymbol{d}_u \\ \boldsymbol{d}_w \end{pmatrix} + \begin{pmatrix} \boldsymbol{0} & \boldsymbol{0} \\ \boldsymbol{C}_{wu} & \boldsymbol{C}_{ww} \end{pmatrix} \begin{pmatrix} \dot{\boldsymbol{d}}_u \\ \dot{\boldsymbol{d}}_w \end{pmatrix} = \begin{pmatrix} \boldsymbol{f}_{ext} \\ \boldsymbol{f}_w \end{pmatrix}, \tag{1.1}$$

where off-diagonal coupling blocks are

$$\boldsymbol{K}_{uw} = -\int_\Omega \boldsymbol{B}_u^{\mathrm{T}} \boldsymbol{m}^{\mathrm{T}} (\alpha S_w) \boldsymbol{N}_w \mathrm{d}\Omega, \qquad \boldsymbol{C}_{wu} = \int_\Omega \boldsymbol{N}_w^{\mathrm{T}} (\alpha S_w) \boldsymbol{m}^{\mathrm{T}} \boldsymbol{B}_u \mathrm{d}\Omega. \tag{1.2}$$

Mašín in [Mašín, 2017] developed the fully-coupled model determined for a material point with suction and temperature as input parameters. The implementation and coupling of this model, together with Lewis and Schrefler's approach, was then implemented as a staggered algorithm. The transport and mechanical parts run separately with data transfer. In this concept, the transport part runs first before the mechanical part. The system of equations (1.1) is modified for the partially coupled approach for transport and mechanical parts separately with the mechanical system of equation rewritten in incremental form

- *Transport part*

$$\boldsymbol{K}_{ww} \boldsymbol{d}_w + \boldsymbol{C}_{ww} \dot{\boldsymbol{d}}_w = \boldsymbol{f}_w + \boldsymbol{f}_{wu}, \tag{1.3}$$

- *Mechanical part*

$$\boldsymbol{K}_{uu}\Delta\boldsymbol{d}_u = \Delta\boldsymbol{f}_u + \Delta\boldsymbol{f}_{uw}, \tag{1.4}$$

where

$$\boldsymbol{f}_{wu} = -\boldsymbol{C}_{wu}\boldsymbol{d}_u = -\int_\Omega \boldsymbol{N}_w^{\mathrm{T}}(\alpha S_w)\boldsymbol{m}^{\mathrm{T}}\boldsymbol{B}_u \mathrm{d}\Omega\boldsymbol{d}_u = -\int_\Omega \boldsymbol{N}^{\mathrm{T}}(\alpha S_w)\Delta\boldsymbol{\varepsilon}_V \mathrm{d}\Omega. \tag{1.5}$$

Vector $\Delta\boldsymbol{\varepsilon}_V$ contains nodal increments of volumetric strains computed from the previous time step. In the presented notation, the right-hand side vector $\Delta\boldsymbol{f}_{uw}$ expresses the forces caused by changes of pore water pressure computed only in the mechanical part from pore water pressure (or suction) increments taken from the transport part

$$\Delta\boldsymbol{f}_{uw} = -\boldsymbol{K}_{uw}\Delta\boldsymbol{d}_w = -\int_\Omega \boldsymbol{B}_u^{\mathrm{T}}\boldsymbol{m}^{\mathrm{T}}(\alpha S_w)\boldsymbol{N}_w \mathrm{d}\Omega\Delta\boldsymbol{d}_w. \tag{1.6}$$

Vector $\Delta\boldsymbol{d}_w$ is the vector of pore water pressure increments. In the hypoplastic model [Mašín, 2013], the vector $\Delta\boldsymbol{f}_{uw}$ is computed from the total stress definition. The vector of total stress $\boldsymbol{\sigma}^{\mathrm{tot}}$ can be expressed in the form of vector function

$$\boldsymbol{\sigma}^{\mathrm{tot}} = \boldsymbol{g}(\boldsymbol{\varepsilon}(\boldsymbol{u}), p^w). \tag{1.7}$$

The time derivative of the stress vector has the form

$$\dot{\boldsymbol{\sigma}}^{\mathrm{tot}} = \frac{\partial \boldsymbol{g}}{\partial \boldsymbol{\varepsilon}}\dot{\boldsymbol{\varepsilon}} + \frac{\partial \boldsymbol{g}}{\partial p^w}\dot{p}^w = \boldsymbol{D}_u\dot{\boldsymbol{\varepsilon}} + \boldsymbol{h}\dot{p}^w. \tag{1.8}$$

The stiffness matrix $\boldsymbol{D}_u$ and vector $\boldsymbol{h}$ are derived from the hypoplastic model [Mašín, 2017]. The extension by the thermal effects is neglected for isothermal processes. The rate of the total stress has to satisfy the equilibrium equation in the form

$$\boldsymbol{\partial}^T\left(\boldsymbol{D}_u\dot{\boldsymbol{\varepsilon}} + \boldsymbol{h}\dot{p}^w\right) + \dot{\boldsymbol{b}} = \boldsymbol{0}. \tag{1.9}$$

Recall, $\dot{\boldsymbol{b}}$ is the time derivative of the body force vector. Additionally, the hypoplastic model involves state variables given by vector $\boldsymbol{p}$ that can also be formulated in the rate form and thus generally, the stress rate can be defined by

$$\dot{\boldsymbol{\tau}} = \boldsymbol{M}\dot{\boldsymbol{\varepsilon}} = \boldsymbol{\Psi}\left(\boldsymbol{\tau}(t), \Delta\boldsymbol{\varepsilon}(t)\right), \tag{1.10}$$

where $\boldsymbol{\tau}$ is the generalized stress vector $\boldsymbol{\tau} = \{\boldsymbol{\sigma}, \boldsymbol{p}\}^T$, $\boldsymbol{M}$ represents the generalized stiffness matrix and $\boldsymbol{\varepsilon}$ is the generalized strain vector $\boldsymbol{\varepsilon} = \{\boldsymbol{\varepsilon}, p^w\}^T$ and $\boldsymbol{\Psi}$ represents the model response function on the given input of strain increment $\Delta\boldsymbol{\varepsilon}$ of the actual time step and attained stress level $\boldsymbol{\tau}$. The explicit integration RKF algorithm with substepping has been selected and implemented in SIFEL. (1.10) represents the initial value problem given by the set of ordinary differential equations. These equations can be written in generic substep k at time interval $[t_n; t_{n+1}]$ formally as follows

$$\boldsymbol{\tau}_{k+1} \;=\; \boldsymbol{\tau}_k + \Delta t_k \sum_{i=1}^{s} b_i\, \boldsymbol{k}_i\left(\boldsymbol{\tau}_k, \Delta\boldsymbol{\varepsilon}(t_{n+1}), \Delta t_k\right), \tag{1.11}$$

where $\boldsymbol{k}_i\left(\boldsymbol{\tau}_k, \Delta\boldsymbol{\varepsilon}(t_{n+1}), \Delta t_k\right)$ represents the function $\boldsymbol{\Psi}$ evaluated for the given strain increment of the actual time step $\Delta\boldsymbol{\varepsilon}(t_{n+1}) = \boldsymbol{\varepsilon}(t_{n+1}) - \boldsymbol{\varepsilon}(t_n)$ and attained stress levels at the prescribed points of the time interval. In Equation (1.11), dimensionless step length $\Delta t_k \in (0; 1]$ has been introduced with the following definition

$$\Delta t_k = \frac{t_{k+1} - t_k}{t_{n+1} - t_n}. \tag{1.12}$$

A detailed description of the integration by Runge-Kutta-Fehlberg methods is presented in the reference [Koudelka et al., 2017].

1.1.2 Benchmark tests

The computer implementation of the hypoplastic model in connection with Lewis and Schrefler's approach [Schrefler and Lewis, 1998] was tested on several examples and benchmarks. Suitable benchmarks can be laboratory tests (Mock ups) of bentonite watering presented in [Hausmannová and Vašíček, 2014] and [Hausmannová, 2017]. These studies focus on the impact of using high hydraulic gradients on combined measurements of hydraulic conductivity and swelling pressure. The hydraulic conditions are supposed to be consistent with possible water pressures in a deep repository. Both parameters are determined in a full saturation state. Measuring these parameters in such a low-permeable bentonite material requires much time. Therefore, the high hydraulic gradients may accelerate the determination of these parameters. Experiments with the Czech bentonite 75 (B75) from Černý vrch deposit were selected for numerical simulations. The material was uniaxially compacted in the laboratory to reach the required dry density $\rho_d = 1200$ to 1750 kg/m^3. The tested samples have a diameter of 30 mm, and a height of 20 mm. The initial values of hydraulic conductivity and swelling pressure were evaluated using a saturation pore water pressure $p^w = 1$ MPa corresponding to the gradient of grad$p^w = 50$ MPa/m (hydraulic gradient 5000) [Hausmannová and Vašíček, 2014]. A unique device was used to measure the hydraulic conductivity and the swelling pressure (Figure 1.1). The setup of this device is described in detail in the reference [Hausmannová and Vašíček, 2014].

The finite element mesh consists of 20 axisymmetric quadrilateral elements in the vertical direction. Linear approximation functions are used in the transport part and quadratic in the mechanical part. The watering process was modeled as a prescribed pore water pressure from the bottom with the values taken from the measurements. Two switching boundary conditions model the top permeable surface. For the first, the water flux is prescribed zero on the boundary until the water head reaches the closest material point, equal to zero water pressure. Then, the conditions are changed to the Dirichlet boundary condition with prescribed zero water pressure. This procedure is commonly used for free soil surface modeling. The initial pore water pressure p_0^w = -100 MPa is set for all benchmarks. The soil parameters used in the simulations are used from the recent calibration for bentonite B75 [Sun et al., 2021]. The sample is fixed to avoid its swelling, and no friction between bentonite material and the steel structure of the testing device is neglected.

Three tests with dry density ρ_d=1298 kg/m^3, ρ_d = 1498 kg/m^3, and ρ_d = 1743 kg/m^3 were used for verification and validation of coupling of mentioned material models in SIFEL computer code and setup of their parameters. A comparison of selected results

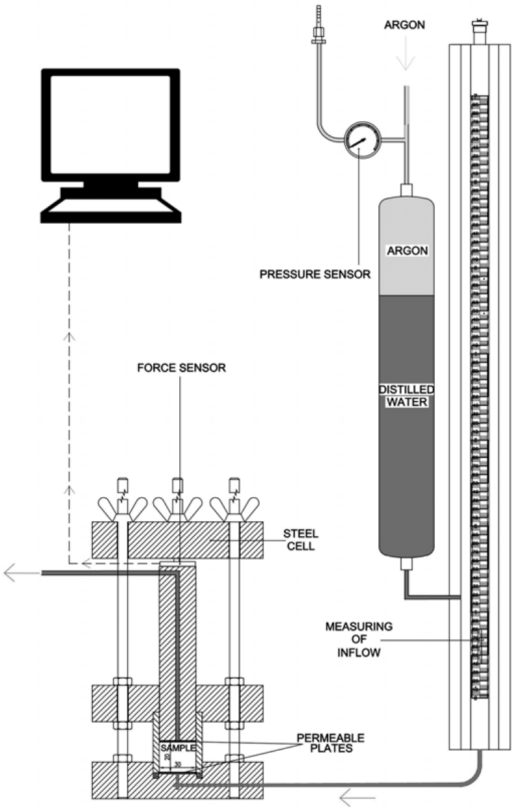

Figure 1.1: Scheme of the measuring device [Hausmannová and Vašíček, 2014].

for different configurations of dry density and hydraulic conductivity is presented. Figures 1.2 and 1.3 show the history of swelling stress for bentonite samples of dry densities $\rho_d = 1498$ kg/m^3 and $\rho_d = 1743$ kg/m^3, respectively. From the considerable amount of computations, the best results closed to the measurements are obtained by using of Bogacki-Shampine integration scheme [Koudelka et al., 2017] for the hypoplastic model in connection with the smoothed water retention curve [Sun et al., 2021] and for maximum time step t_{max}=1000 s [Scaringi et al., 2022]. It has to be mentioned that such numerical simulations are strongly non-linear, time step length-dependent, and time-consuming. Most of them took from 10 to 20 hours, despite the use of multithreading architecture via OpenMP system.

Attained levels of swelling pressure at full saturation depend only on the setup of initial dry densities. This fact corresponds to the previous experiments and hypoplastic model calibration. The swelling stress for bentonite with $\rho_d = 1498$ kg/m^3 is about 3 MPa, and for $\rho_d = 1743$ kg/m^3 is 10.5 MPa, respectively. The initial swelling pressures growth is influenced by the sample saturation rate, related to intrinsic permeability (or hydraulic conductivity). The permeability was assumed constant for all benchmarks. For better compliance with the measurements in the initial phase, the application of a relationship dependent on saturation degree can be successfully used. The coincidence between simulations and measurements is validated as relatively good. The trends of watering with loading water pressure jumps are captured well.

From the analysis of the results, it can be concluded that coupling the hypoplastic

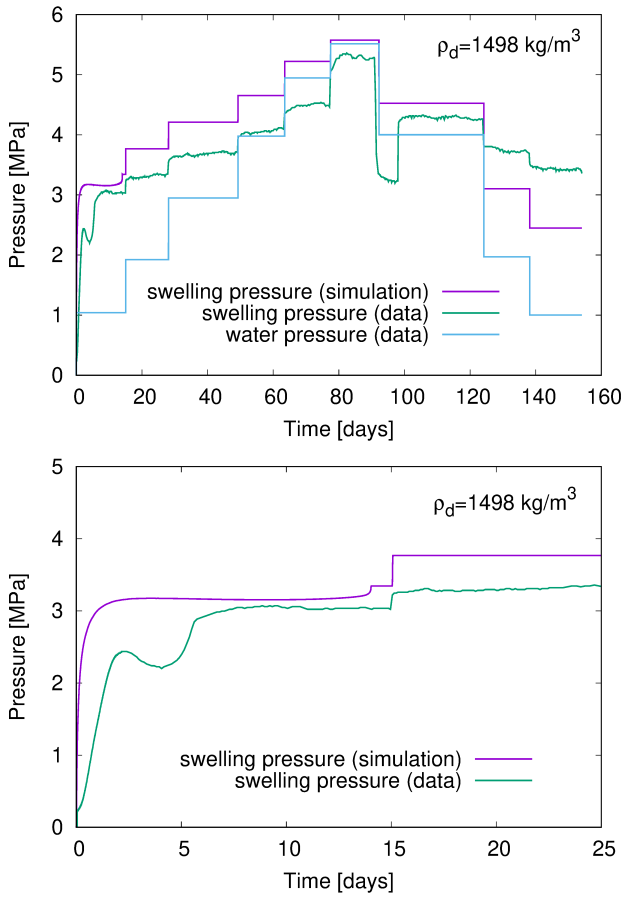

Figure 1.2: History of water pressure and swelling pressure for bentonite B75 $\rho_d = 1498$ kg/m^3 and $K^w = 2.0{\cdot}10^{-13}$ m/s [Scaringi et al., 2022] (left), and zoom of the initial phase (right).

model in connection with Lewis and Schrefler's approach in a staggered scheme works well. However, the model response is primarily dependent on the hypoplastic model setup.

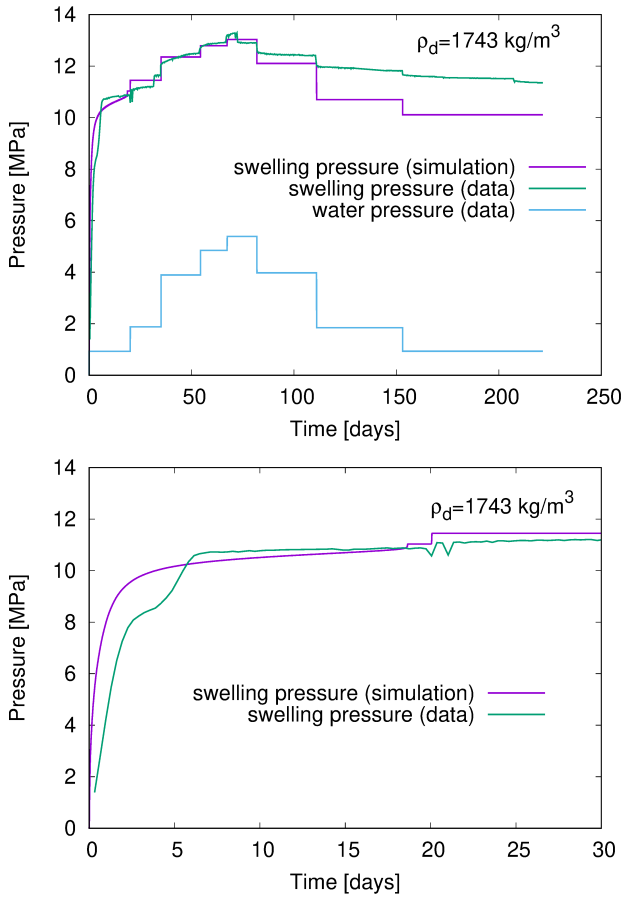

Figure 1.3: History of water pressure and swelling pressure for bentonite B75 $\rho_d = 1743$ kg/m^3 and $K^w = 1.0{\cdot}10^{-13}$ m/s [Scaringi et al., 2022], and zoom of the initial phase (right).

Bibliography

[Hausmannová, 2017] Hausmannová, L. (2017). *The influence of water pressure on the hydraulic conductivity and swelling pressure of Czech bentonites*. PhD thesis, Czech Technical University in Prague. In Czech.

[Hausmannová and Vašíček, 2014] Hausmannová, L. and Vašíček, R. (2014). Measuring hydraulic conductivity and swelling pressure under high hydraulic gradients. *Geological Society London Special Publications*, 400.

[Koudelka et al., 2017] Koudelka, T., Krejčí, T., and Kruis, J. (2017). Coupled hydro-mechanical model for expansive clays. *AIP Conference Proceedings*, 1863(1):290008.

[Mašín, 2013] Mašín, D. (2013). Double structure hydromechanical coupling formalism and a model for unsaturated expansive clays. *Engineering Geology*, 165:73–88.

[Mašín, 2017] Mašín, D. (2017). Coupled thermohydromechanical double-structure model for expansive soils. *Journal of Engineering Mechanics*, 143(9).

[Scaringi et al., 2022] Scaringi, G., Mašín, D., Najser, J., Sun, H., and Sun, Z. (2022). Thermo-hydro-mechanical hypoplastic modelling of bentonite buffers for nuclear waste disposal: model calibration and performance. In *In preparation for Proceedings of the 20th International Conference on Soil Mechanics and Geotechnical Engineering, Sydney 2022*.

[Schrefler and Lewis, 1998] Schrefler, B. A. and Lewis, R. W. (1998). *The Finite Element Method in the Static and Dynamic Deformation and Consolidation of Porous Media*. 2nd Edition. John Wiley & Sons.

[Sun et al., 2021] Sun, H., Scaringi, G., Mašín, D., and Najser, J. (2021). An experimental investigation on the swelling behavior of compacted b75 bentonite. *Engineering Geology*, page 106452.